A Unique Molten Globule State Occurs during Unfolding of Cytochrome *c* by $LiClO_4$ Near Physiological pH and Temperature: Structural and Thermodynamic Characterization†

Beenu Moza,‡ Shabir Hussain Qureshi,‡ Asimul Islam,‡ Rajendrakumar Singh,‡ Farah Anjum,‡ Ali Akbar Moosavi-Movahedi,§ and Faizan Ahmad*,‡

Department of Biosciences, Jamia Millia Islamia, Jamia Nagar, New Delhi, 110 025, India, and Institute of Biochemistry and Biophysics, University of Tehran, Tehran, Iran

Received November 18, 2005; Revised Manuscript Received February 13, 2006

ABSTRACT: We have carried out denaturation studies of bovine cytochrome *c* (cyt *c*) by $LiClO_4$ at pH 6.0 and 25 °C by observing changes in difference molar absorbance at 400 nm ($\Delta\epsilon_{400}$), mean residue ellipticities at 222 nm ($[\theta]_{222}$) and difference mean residue ellipticity at 409 nm ($\Delta[\theta]_{409}$). The denaturation is a three-step process when measured by $\Delta\epsilon_{400}$ and $\Delta[\theta]_{409}$, and it is a two-step process when monitored by $[\theta]_{222}$. The stable folding intermediate state has been characterized by near- and far-UV circular dichroism, tryptophan fluorescence, 8-anilino-1-naphthalene sulfonic acid (ANS) binding, and intrinsic viscosity measurements. A comparison of the conformational and thermodynamic properties of the $LiClO_4$-induced molten globule (MG) state with those induced by other solvent conditions (e.g., low pH, LiCl, and $CaCl_2$) suggests that $LiClO_4$ induces a unique MG state, i.e., (i) the core in the $LiClO_4$-induced state retains less secondary and tertiary structure than that in the MG states obtained in other solvent conditions, and (ii) the thermodynamic stability associated with the $LiClO_4$-induced process, native state ↔ MG state, is the same as that observed for each transition between native and MG states induced by other solvent conditions.

The process of protein folding, while critical and fundamental to virtually all of biology, remains a mystery. It is important to elucidate the hierarchy of interactions that stabilize the native state. Characterization of folding intermediates provides an insight into the understanding of how and when different forces come into play to direct protein folding. The development of a broad range of techniques has led to the identification and characterization of stable intermediates in several proteins (*1*−*4*). One such stable intermediate state termed the molten globule (MG[1]) has been shown to be a compact collapsed structure that has pronounced secondary structure but largely disordered tertiary structure (*5*, *6*). Some structural similarities between the MG and native states of proteins also seem to have a significant bearing on understanding the protein folding problem (*7*).

The molten globule state of cytochrome *c* (cyt *c*) can be induced at low pH values (called acidic MG) by reducing the electrostatic repulsions (*8*, *9*) and near neutral pH upon unfolding by weak salt denaturants (*10*). The acidic MG state has been extensively investigated, and, therefore, the conformation, stability, and mechanism of stabilization have been understood in great detail (*1*−*9*). A broad body of information on conformation of MG state of various proteins reveals that this intermediate has a large pool of conformational variations (*5*, *6*, *8*, *11*, *12*). This has raised new questions regarding how many intermediates can be covered by the term MG. Contrary to the data available on acidic MG, there are very few reports available in the literature about the MG state induced at or near physiological pH (*10*, *13*, *14*). It may be noted that the MG state of a protein is also shown to be present in the living cells where they are involved in many physiological processes (*5*, *6*). Thus, the MG generated at a low pH condition may bear little relevance to the MG state found inside cells at physiological pH. It is therefore necessary to characterize extensively the MG states near neutral pH and understand the interactions that stabilize them at physiological pH. This will enhance our understanding not only of protein folding in vitro and in vivo but also of many cellular processes such as protein translocation or protein recognition by chaperones.

In an attempt to characterize the molten globule states generated at physiological pH, we have been carrying out systematic studies of the denaturation of cyt *c* by weak salt denaturants. In our earlier communication (*10*), we have shown that MG states generated by LiCl and $CaCl_2$ have similar conformational and thermodynamic properties. In this study we have investigated the denaturation of cyt *c* by $LiClO_4$ at pH 6.0 and compared the results with those obtained from the LiCl-induced and $CaCl_2$-induced de-

† This work was supported by Grant 37(1078) 01/EMR-II from the Council of Scientific and Industrial Research, India.

* Corresponding author. Tel: +91-11-2698 1733. Fax: +91-11-2698 1232. E-mail: faizan_ahmad@yahoo.com.

‡ Jamia Millia Islamia.

§ University of Tehran.

[1] Abbreviations: CD, circular dichroism; ϵ, molar absorption coefficient; $\Delta\epsilon_{400}$, difference molar absorbance at 400 nm; $[\theta]_{222}$, mean residue ellipticity at 222 nm; $\Delta[\theta]_{409}$, difference mean residue ellipticity at 409 nm; ANS, 8-anilino-1-naphthalene sulfonic acid; cyt *c*, cytochrome *c*; MG, molten globule; y_N, optical property of the native state; y_D, optical property of the denatured state; GdnHCl, guanidine hydrochloride.

10.1021/bi052357r CCC: $33.50
Published on Web 03/18/2006

naturations (*10*). We report that (i) $LiClO_4$ induces the MG state that exists on the folding/unfolding pathway, (ii) the $LiClO_4$-induced MG state retains less native secondary and tertiary structure than that induced by LiCl and $CaCl_2$, and (iii) the thermodynamic stability of the $LiClO_4$-induced MG state is the same as that of the $CaCl_2$-induced and LiCl-induced MG states.

MATERIALS AND METHODS

Commercially lyophilized chromatographically purified bovine cytochrome*c* (cyt *c*) was purchased from Sigma Chemical Co. Since protein gave a single band on SDS−PAGE, it was used without further purification. Lithium perchlorate, sodium salt of cacodylic acid, and 8-anilino-1-naphthalene sulfonic acid (ANS) were also purchased from Sigma Chemical Co. NaCl was purchased from Merck (India). These and other chemicals were analytical-grade reagents and used without further purification.

Preparation of Solutions. Cyt *c* was oxidized first by adding 0.01% potassium ferricyanide as described earlier (*15*). The concentration of the oxidized cyt *c* was determined experimentally using a value of 106 000 M^{-1} cm^{-1} for the molar absorption coefficient (ϵ) at 409 nm (*16*). The concentration of the stock solution of ANS was determined spectrophotometrically using a value of 5000 M^{-1} cm^{-1} for ϵ at 350 nm (*17*). For optical measurements all solutions were prepared in 0.03 M cacodylate buffer containing 0.1 M NaCl at pH 6.0 and incubated overnight at room temperature.

Absorbance and CD Measurements. Isothermal denaturation of cyt *c* by $LiClO_4$ at 25.0 ± 0.1 °C was measured in a Shimadzu 2100 UV/vis spectrophotometer and in a Jasco spectropolarimeter (model J-715) equipped with a Peltier-type temperature controller (PTC-348 WI). Protein concentration used for the absorption measurements was in the range 7−10 μM, and that for the CD measurements was in the range 18−20 μM. Cells of 0.1 and 1.0 cm path length were used for the measurements of the far- and near-UV spectra, respectively. The CD instrument was routinely calibrated with D-10-camphorsulfonic acid. The results of all the CD measurements are expressed as mean residue ellipticity ($[\theta]_\lambda$) in deg cm^2 $dmol^{-1}$ at a given wavelength λ (nm) using the relation

$$[\theta]_\lambda = \theta_\lambda M_o/10cl \qquad (1)$$

where θ_λ is the observed ellipticity in millidegrees at wavelength λ, M_o is the mean residue weight of the protein, c is the protein concentration (mg/cm^3), and l is the path length (cm). It should be noted that each observed θ_λ of the protein was corrected for the contribution of the solvent. Reversibility of the isothermal denaturation by $LiClO_4$ was checked using the procedure described earlier (*18*). Reversibility of the thermal denaturation was checked by matching the optical properties before and after the denaturation.

Fluorescence Measurements. Fluorescence spectra were measured in a Perkin-Elmer L-5 spectroluminescence meter in a 5 mm quartz cell at 25 °C, with both excitation and emission slits set at 12 nm. Protein concentration for all the experiments was in the range 7−10 μM. For the ANS fluorescence in ANS−protein binding experiments the excitation wavelength was 360 nm, and emission spectra were recorded from 600 to 400 nm. For tryptophan florescence measurements the excitation wavelength was 282 nm, and emission spectra were recorded in the wavelength region 300−400 nm.

Viscosity Measurements. Viscosity measurements were carried out in an Oswald type viscometer with a flow rate of 60 s for 1 mL of distilled water. Viscometer was kept in a thermostated water bath to maintain the temperature of samples at 25.0 ± 0.1 °C. Protein concentration used was in the range 2.0−25.0 mg mL^{-1}. As described earlier (*19*), the reduced viscosity (η_{red}) of the protein was determined at different protein concentrations using the relation

$$\eta_{red} = (t - t_o)/t_o c + (1 - \bar{v}_2\rho_o)/\rho_o \qquad (2)$$

where t_o and t are the times of fall of 1 mL each of the solvent and protein solution, respectively, c is the protein concentration in g mL^{-1}, $\bar{v}_2$ is the partial specific volume of cyt *c* which is 0.724 mL g^{-1} (*20*), and ρ_o is the density of the solvent.

RESULTS

To understand the unfolding mechanism of cyt *c* in the presence of $LiClO_4$, we have studied $LiClO_4$-induced denaturation of the protein by observing changes in the absorption at 400 nm and in circular dichroism (CD) at 222 and 409 nm at pH 6.0 and 25 °C. The unfolding profiles are presented in Figure 1A−C. It can be seen in Figures 1A and 1C that the denaturation transitions monitored by $\Delta\epsilon_{400}$ and $\Delta[\theta]_{409}$ are composed of two distinct processes. The first transition is centered in the [$LiClO_4$], molar concentration of $LiClO_4$, range 0−1.85 M and is represented here by the reaction N ↔ X, where X is the thermodynamically stable intermediate state of the protein between its N (native) and D (denatured) states. The second transition occurs in the [$LiClO_4$] range 1.85−3.3 M and is represented here by the reaction X ↔ D. It is also seen in Figure 1B that there is no change in $[\theta]_{222}$ in the [$LiClO_4$] range corresponding to the N ↔ X transition monitored by $\Delta[\theta]_{409}$ (Figure 1C) and $\Delta\epsilon_{400}$ (Figure 1A). Figure 1 also shows that y_N (optical property of the native state) and y_D (optical property of the denatured state) are well defined, and their dependencies on [$LiClO_4$] were determined by fitting the data in the pre- and posttransition regions, respectively, using linear least-squares analysis. Solid lines shown in Figure 1 depict the [$LiClO_4$] dependence of y_N and y_D. It is also seen in Figure 1A that the X state exists in a very narrow concentration range, and the dependence of y_X on [$LiClO_4$] cannot be determined from these results. For the determination of the [$LiClO_4$] dependence of y_X, we have used the procedure described earlier for LiCl- and $CaCl_2$-induced denaturations (*10*). That is, we have carried out heat-induced denaturation of cyt *c* in the presence of $LiClO_4$ in the concentration range 1.25−1.70 M. All heat-induced denaturation curves in the presence of a fixed [$LiClO_4$] in this range were biphasic, N ↔ X ↔ D (results not shown). It was also observed that the absorption property of the X state is independent of temperature and depends on [$LiClO_4$] only (see inset in Figure 1A). This dependence of y_X on [$LiClO_4$] is shown by a straight line in Figure 1A. The inset in Figure 1C shows the [$LiClO_4$] dependence of

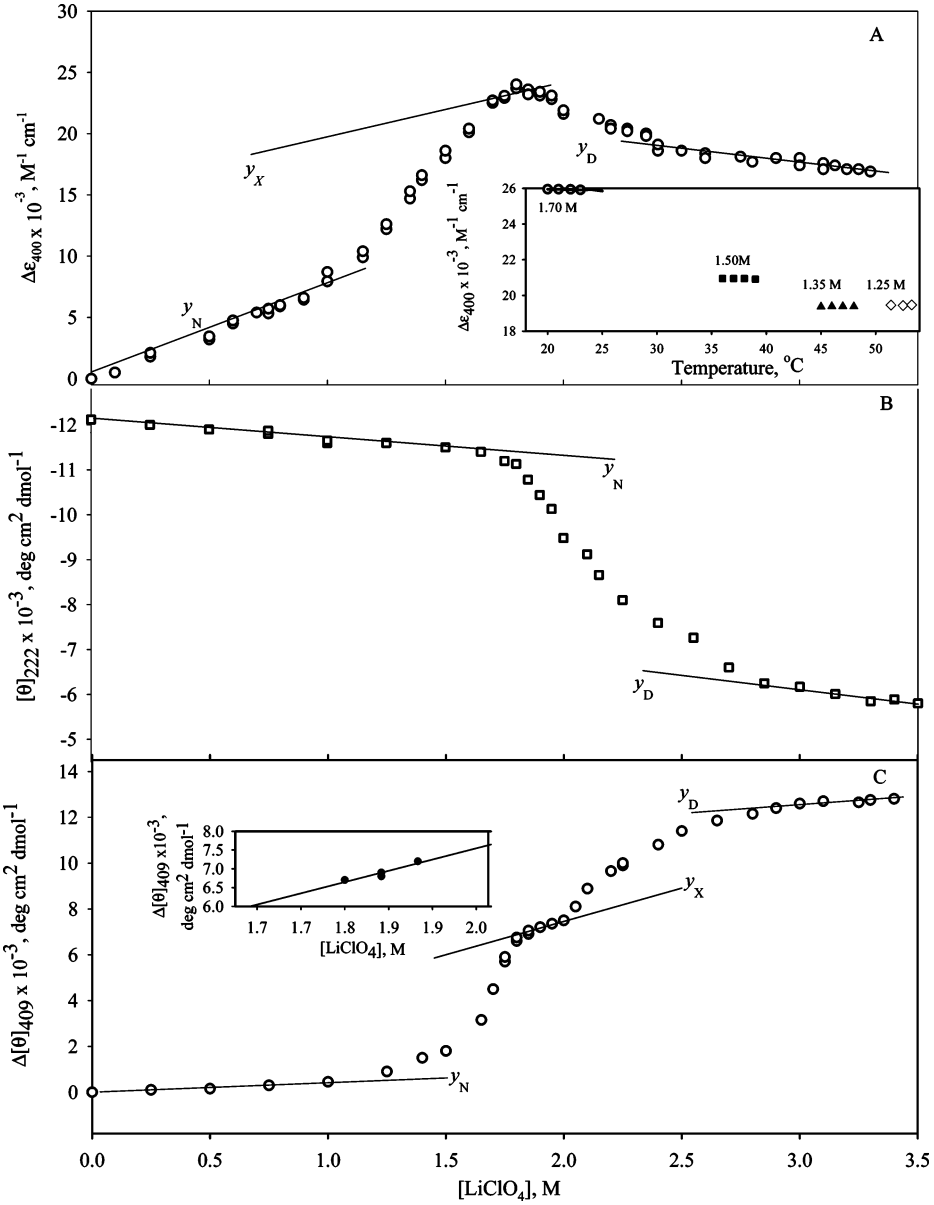

FIGURE 1: $LiClO_4$-induced denaturation curves of cyt *c* at pH 6.0 and 25 °C. Denaturation curves were measured by observing changes in $\Delta\epsilon_{400}$ (A), $[\theta]_{222}$ (B), and $\Delta[\theta]_{409}$ (C). Inset in panel A shows the temperature dependence of the optical property of X state (y_X) on $[LiClO_4]$. Inset in panel C shows the plot for the dependence of the optical property of the X state (y_X) on $[LiClO_4]$ on the expanded scale.

the CD at 409 nm of the X state of the protein. It has been observed that both transitions, N ↔ X and X ↔ D, are reversible.

Assuming that the process N ↔ X, designated here as transition I, follows a two-state mechanism, results shown in Figures 1A and 1C were used to determine values of f_I (fraction of molecules in the intermediate state) and ΔG_I (Gibbs energy change associated with the transition I) using the relations

$$f_I = (y - y_N)/(y_X - y_N) \quad (3A)$$

$$\Delta G_I = -RT \ln[(y - y_N)/(y_X - y)] \quad (3B)$$

where R is the universal gas constant, T is the temperature in kelvins, and y is the observed optical property corresponding to transition I. Values of f_I and those of ΔG_I in the range $-1.3 \leq \Delta G_I$, kcal $mol^{-1} \leq 1.3$ are plotted as a function of $[LiClO_4]$ in Figure 2. The ΔG_I versus $[LiClO_4]$ plot was analyzed for ΔG_I^0 (ΔG_I value at zero $[LiClO_4]$) and m_I, the slope ($\delta\Delta G_I/\delta[LiClO_4]$), using the relation

$$\Delta G_I = \Delta G_I^{\,0} - m_I\,[LiClO_4] \quad (4)$$

Table 1 shows the values of ΔG_I^0, m_I, and C_{mI}, the midpoint of the transition I ($=\Delta G_I^0/m_I$).

Assuming that the process X ↔ D, designated here as transition II, is also of a two-state type, results shown in Figures 1A−1C were used to determine values of f_{II} (fraction of molecules in the D state) and ΔG_{II} (Gibbs energy change associated with transition II) using the relations

$$f_{II} = (y - y_X)/(y_D - y_X) \quad (5A)$$

$$\Delta G_{II} = -RT \ln[(y - y_X)/(y_D - y)] \quad (5B)$$

where y is the observed optical property corresponding to transition II and y_D is the optical property of the denatured

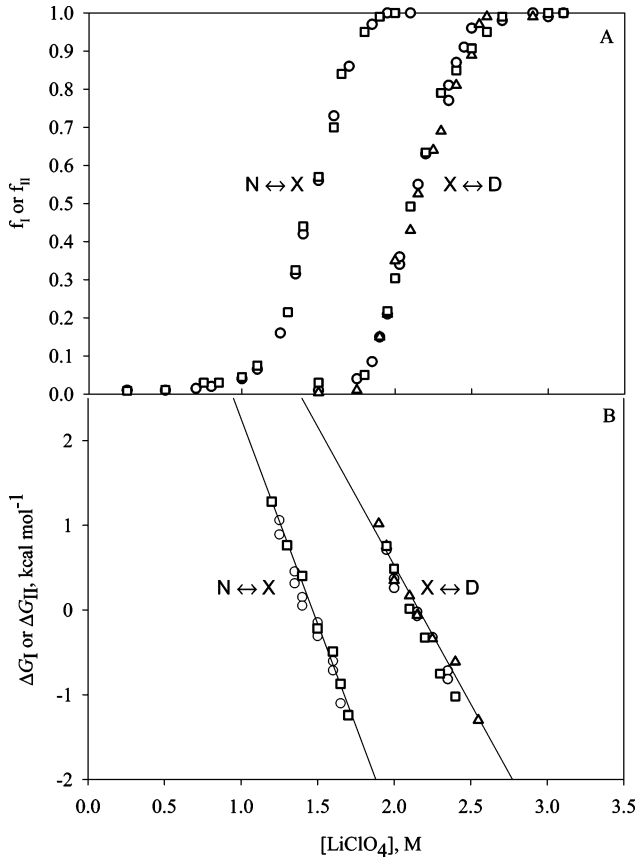

FIGURE 2: Normalized transition curves and ΔG_I and ΔG_{II} versus [LiClO$_4$] plots. The change in the fraction, obtained by observing changes in $\Delta\epsilon_{400}$ (○), $[\theta]_{222}$ (△), and $\Delta[\theta]_{409}$ (□), is plotted as a function of [LiClO$_4$] in A. Plots of ΔG_I and ΔG_{II} versus [LiClO$_4$] are shown in B. Symbols in panel B have the same meanings as in panel A.

Table 1: Thermodynamic Parameters Characterizing the LiClO$_4$ Denaturations of Cyt *c* at pH 6.0 and 25 °C

Probe	transition	$\Delta G_I^0/\Delta G_{II}^X$,[a] kcal mol^{-1}	m_I/m_{II}, kcal mol^{-1} M^{-1}	C_{mI}/C_{mII}, M
$\Delta\epsilon_{400}$	N ↔ X	9.6 ± 0.5	−6.2 ± 0.1	1.5 ± 0.1
	X ↔ D	1.2 ± 0.3	−3.6 ± 0.2	2.2 ± 0.1
$\Delta[\theta]_{409}$	N ↔ X	9.5 ± 0.4	−6.1 ± 0.2	1.5 ± 0.1
	X ↔ D	1.1 ± 0.3	−3.7 ± 0.2	2.2 ± 0.1
$[\theta]_{222}$	N ↔ X			
	X ↔ D	1.6 ± 0.2	−4.4 ± 0.2	2.3 ± 0.1

[a] ΔG_{II}^X is the value of ΔG_{II} at [LiClO$_4$] where the X state exists.

protein molecule. Figure 2A shows the plot of f_{II} versus [LiClO$_4$]. Values of ΔG_{II} in the range $-1.3 \leq \Delta G_{II}$, kcal mol$^{-1} \leq 1.3$ are plotted as a function of [LiClO$_4$] in Figure 2B, where it is seen that the plot of ΔG_{II} versus [LiClO$_4$] is linear. A linear least-squares analysis was used to obtain values of ΔG_{II}^0 and m_{II} using the relation

$$\Delta G_{II} = \Delta G_{II}^{\ 0} - m_{II}[\mathrm{LiClO_4}] \qquad (6)$$

where subscript II represents the fact that these parameters correspond to transition II, and superscript "0" represents the value at 0 M LiClO$_4$. Values of ΔG_{II}^X, the value of ΔG_{II} at 1.8 M LiClO$_4$, m_{II}, and $C_{m\ II}$ ($=\Delta G_{II}^0/m_{II}$) are given in Table 1.

Figures 3A and 3B show respectively the far- and near-UV CD spectra of cyt *c* in the native (curve 1), LiClO$_4$-induced intermediate (curve 2) and LiClO$_4$-induced denatured (curve 3) states. These figures also show the CD spectra of MG states induced by LiCl at pH 6.0 (curve 4) and NaCl at acidic pH (curve 5), which are in excellent agreement with those reported earlier (*8*, *10*). It can be seen in Figure 3B that the near-UV CD spectrum of the LiClO$_4$-induced X state is similar to that of the LiClO$_4$-induced D state, and the characteristic negative peaks at 282 and 289 nm of the native protein that arise from the tyrosyl side chains (*12*) are absent in both X and D states. This figure also shows the near-UV CD spectra of MG states induced by LiCl (pH 6.0) and 0.25 M NaCl (pH 2.0), which are in excellent agreement with those reported earlier (*8*, *10*). A comparison of these CD spectra of the protein with that of the guanidine hydrochloride (GdnHCl) denatured protein (*10*) reveals that the extent of exposure of aromatic amino acid residues is almost the same in the GdnHCl-denatured state and LiClO$_4$-induced X and D states.

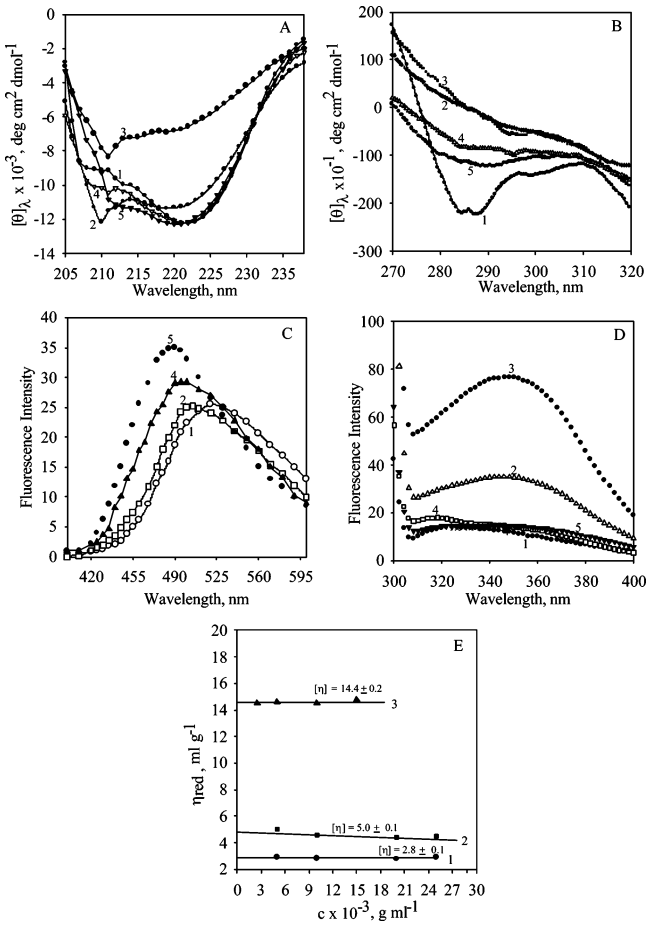

FIGURE 3: Structural characterization of various states of cyt *c*. Measurements of the far- (A) and near-UV (B) CD, ANS fluorescence (C), Trp fluorescence (D), and reduced viscosity (E) at 25 °C. Curve numbers 1, 2, 3, 4, and 5 represent the native state, LiClO$_4$-induced MG state, LiClO$_4$-induced denatured state, LiCl-induced MG state, and acid-induced MG state, respectively.

Figure 3C shows the ANS fluorescence when it is added to cyt *c* in the native (curve 1) and the LiClO$_4$-induced X state (curve 2). The excitation was carried out at 365 nm, and emission was recorded in the range 400−600 nm. It is seen in Figure 3C that the fluorescence of ANS in the presence of the protein existing in the X state is accompanied by a blue shift with respect to the native state. It should be noted that fluorescence measurements in the presence of a

$LiClO_4$ concentration that gives the D state could not be carried out due to insolubility of ANS in high $LiClO_4$ concentrations. Figure 3C also shows the ANS fluorescence spectra of the MG state induced by LiCl at pH 6.0 (curve 4) and NaCl at low pH (curve 5). These observations are in excellent agreement with those reported earlier (*10*).

Figure 3D shows the Trp fluorescence spectra of cyt *c* in the native (curve 1) and $LiClO_4$-induced thermodynamically stable intermediate (curves 2) states. This figure also shows the emission spectra of MG states of cyt *c* induced by 5.9 M LiCl at pH 6.0 (curve 4) and by 0.25 M NaCl at pH 2.0 (curve 5). Trp fluorescence spectra of both the native and 0.25 M NaCl-induced MG states are in agreement with those reported earlier (*21*, *22*).

Figure 3E shows plots of reduced viscosity (η_{red}) versus concentration (*c*) of cyt *c* in the native (curve 1), intermediate (X) (curve 2), and denatured (curve 3) states. A linear least-squares analysis of these plots gave the values of intrinsic viscosity ([η]), the value of η_{red} at $c = 0$. It can be seen in Figure 3E that the value of [η] increases from 2.80 ± 0.11 mL g^{-1} for the native protein to values of 4.98 ± 0.11 mL g^{-1} for the X state and 14.4 ± 0.2 mL g^{-1} for the D state. It should be noted that [η] of the native protein is in excellent agreement with those reported earlier (*9*, *10*, *21*).

DISCUSSION

The reversible unfolding profiles of cyt *c* monitored by $\Delta\epsilon_{400}$ and $\Delta[\theta]_{409}$ measurements, presented in Figures 1A and 1C, are biphasic (N ↔ X ↔ D). This equilibrium study of denaturation provides direct evidence of the presence of a stable folding intermediate at neutral pH, which gets populated in an extremely narrow range of [$LiClO_4$]. A comparison of denaturation curves monitored by $\Delta\epsilon_{400}$ (Figure 1A) and $\Delta[\theta]_{409}$ (Figure 1C) with that monitored by $[\theta]_{222}$ (Figure 1B) reveals that there is very little change in the peptide CD in the denaturant concentration range in which transition I (N ↔ X) is observed; values of $[\theta]_{222}$ are −12 200 and −11 100 for the protein in the N and X states, respectively (Table 2). This comparison suggests that the stable folding intermediate state X populated around 1.85 M $LiClO_4$ has one of the structural characteristics of the MG state, namely, the presence of most of the secondary structure that the native protein originally had (*5*).

The presence of exposed hydrophobic clusters and its binding with hydrophobic dyes such as ANS is one of the properties of MG state (*5*). It has been reported that ANS shows an increase in the fluorescence intensity with a blue shift in the emission maximum on binding with proteins in the molten globule state (*5*). We have successfully exploited this observation in the characterization of the MG state of cyt *c* induced by LiCl, $CaCl_2$, and NaCl at low pH (*10*). To ascertain whether the X state of cyt *c* induced by $LiClO_4$ has MG-like character, we have carried out fluorescence measurements of ANS in the presence of the protein. Our observation suggests that there is a blue shift in the emission maximum of ANS in the presence of the protein in the X state without any change in the fluorescence intensity at the wavelength of emission maximum (Figure 3C). As argued earlier (*26*, *27*), no increase in the fluorescence intensity of the X state induced by $LiClO_4$ may be due to the extensive melting of the tertiary structure, leading to large conformational freedom. These fluorescence results suggest that the X state has a MG characteristic, namely, a loosely packed hydrophobic core that increases the hydrophobic surface exposed to the solvent (*5*, *6*). Another known characteristic of the MG state is the absence of most of the specific tertiary structure produced by tight packing of side chains in the native protein (*5*, *6*, *21*). It is seen in Figure 3B that the near-UV CD spectrum of cyt *c* in the presence of 1.85 M $LiClO_4$ (curve 2) is nearly the same as that of the denatured state induced by 3.3 M $LiClO_4$ (curve 3). This observation suggests that the X state has lost most of its native tertiary interactions involving aromatic amino acid residues.

Table 2: Structural and Thermodynamic Properties of Various Molten Globule States of Cyt *c* at 25 °C

property	$LiClO_4$	LiCl	acid
$[\theta]_{222}$, deg cm^2 dmol^{-1}	−11100	−12200	−12100
$[\theta]_{287}$, deg cm^2 dmol^{-1}	−7	−85	−119
$[\theta]_{416}$, deg cm^2 dmol^{-1}	−6700	−4500	−4500[a]
ANS fluorescence intensity at λ_{max}	25.2	29.2	35.0
Trp fluorescence intensity at λ_{max}	34.9	14.2	14.6
R_G, Å	17	15[b]	15[c]
ΔG_I^0, kcal mol^{-1}	9.6	9.5[b]	9.0[d]
ΔG_{II}^0, kcal mol^{-1}	1.3	1.5[b]	2.8[e]

[a] Taken from ref *8*. [b] Taken from ref *10*. [c] As described in the text, R_G value calculated from the [η] reported in ref *23*. [d] Value estimated using Gibbs−Helmholtz equation with the reported values ($T_m = 83$ °C, $\Delta H_m = 107$ kcal mol^{-1}, and $\Delta C_p = 1.38$ kcal mol^{-1} K^{-1}) given in ref *24*. [e] Value estimated using Gibbs−Heltmholtz equation with the reported values ($T_m = 36$ °C, $\Delta H_m = 57$ kcal mol^{-1}, and $\Delta C_p = 1.12$ kcal mol^{-1} K^{-1}) given in ref *25*.

To further characterize the X state, intrinsic viscosities of N, X, and D states of cyt *c* were measured under appropriate experimental conditions (see Figure 3E). [η] is a measure of the hydrodynamic volume and hence the hydrodynamic radius (R_h). For a solid sphere R_h is related to R_G, the radius of gyration, through the relation $R_G = 3(Re)^2/5$ (see eq 18−20 in ref *28*). We have estimated R_G values of the native and X (Table 2) states and found that the X state in terms of radius of gyration is about 22% less compact than the native state. All the structural characterizations of the stable folding intermediate state X of cyt *c* induced by $LiClO_4$ led us to conclude that this state has all the common characteristics of the molten globule state (*5*), namely, (i) the presence of a pronounced amount of secondary structure, (ii) the absence of most of the specific tertiary structure produced by tight packing of side chains, (iii) compactness of the protein molecule with a radius of gyration 10−30% larger than that of the native state, and (iv) the presence of a loosely packed hydrophobic core that increases the hydrophobic surface accessible to the solvent.

Various MG-like thermodynamically stable intermediates have been observed in cyt *c* (*29*). Kuroda et al. (*25*) have reported a state called IIc, which has MG-like characteristics in 0.5 M KCl at pH 2.0, and moderately high temperatures (55−60 °C). The addition of neutral sugars or sugar alcohols to the acid unfolded cyt *c* also induces a MG-like thermodynamically stable intermediate (*29*, *30*). Bai et al. (*31*) have shown by hydrogen exchange experiments on cyt *c* at low GdnHCl concentrations that the MG-like intermediates are transiently populated under native conditions. A MG state of cyt *c* can also be induced near neutral pH upon denaturation by weak salt denaturants (LiCl and $CaCl_2$) (*10*).

Furthermore, the addition of a stabilizing anion from the salt or acid to the acid-unfolded cyt *c* transforms it into a compact thermodynamically stable intermediate that has MG characteristics (*5*). It may be noted that only NaCl- (pH 2.0), LiCl- (pH 6.0), and $CaCl_2$- (pH 6.0) induced MG states are the well-characterized ones, for the structure and thermodynamics of these MG states are extensively studied. We shall, however, compare the $LiClO_4$-induced MG state (pH 6.0) with only NaCl- (pH 2.0) and LiCl- (pH 6.0) induced MG states, for MG states induced by $CaCl_2$ and LiCl at pH 6.0 and 25 °C are shown to have identical structural and thermodynamic properties (*10*).

A comparison of the far- and near-UV CD spectra, ANS fluorescence, and Trp fluorescence of the $LiClO_4$-induced MG state with those of LiCl- and NaCl-induced states reveals several interesting features. It is seen in Figure 3A that the helical content of the MG obtained at 1.85 M $LiClO_4$ (curve 2) is slightly less than those MG states induced by 5.9 M LiCl at pH 6.0 (curve 4) and by 0.25 M NaCl at pH 2.0 (curve 5). It is also seen in this figure that the helical content of the native protein is retained in the latter two MG states. It has been argued that the hydrophobic core composed of main helix segments of the native protein is retained in the acid MG state (*32*, *33*). It is tempting to suggest that such helical segments are slightly perturbed in the $LiClO_4$-induced MG state but maintained in the LiCl-induced MG state. It is seen in Figure 3B that the aromatic tertiary interactions in the MG state induced by $LiClO_4$ (curve 2) are much less than those in the LiCl-induced (curve 4) and NaCl-induced MG (curve 5) states. In fact, the loss of such tertiary interactions in the $LiClO_4$-induced MG state is almost the same as that in the D states obtained in concentrated solutions of $LiClO_4$ (curve 2 and 3 in Figure 3B). These results show that the exposure of the aromatic side chains in the $LiClO_4$-induced MG state is different from that in the MG states induced by LiCl and NaCl. The ANS fluorescence emission spectra of MG states of cyt *c* induced by $LiClO_4$ at pH 6.0 (curve 2), NaCl at pH 2.0 (curve 5), and LiCl at pH 6.0 (curve 4) also show that the $LiClO_4$-induced MG state is structurally different from those induced by LiCl and NaCl.

Cyt *c* has a single Trp residue at position 59 that is approximately at a distance of 1 Å from the heme (*33*). This heme−Trp distance is largely maintained in the acid MG state of cyt *c* (*34*). Trp−heme forms an energy donor acceptor pair (*8*). The fluorescence of Trp is completely quenched in the native cyt *c* due to resonance energy transfer to the adjacent heme group, and quenching of Trp fluorescence decreases with the increasing distance between heme and Trp (*8*). Thus, Trp fluorescence quenching is a sensitive method of monitoring the gross conformational change in this protein. In order to compare the heme−Trp distance in the $LiClO_4$-induced MG state with that in MG states induced by LiCl (pH 6.0) and NaCl (pH 2.0), Trp fluorescence of all the three MG states as well as the native state were measured (Figure 3D). As observed earlier (*26*), the fluorescence spectrum of the native state is the same as that of the acid MG state. It has been argued that the heme−Trp distance in the native protein is largely maintained in the acid MG state (*21*, *35*). In our experiments (Figure 3D) the Trp fluorescence spectrum of the native protein (curve 1) is also similar to that of the MG state induced by LiCl at pH 6.0 (curve 4), suggesting that the heme−Trp distance in the native protein is also not perturbed in the LiCl-induced MG state. On the other hand, there is an increase in Trp fluorescence of the $LiClO_4$-induced MG state (curve 3 in Figure 3D), suggesting that the quenching efficiency has been reduced most probably as a result of increase in distance between heme and Trp (*8*). Thus, either the loss of aromatic tertiary interactions (curve 2 in Figure 3B) or some secondary structural elements (curve 2 in Figure 3A) or both have a destabilizing effect on the structural integrity as well as the heme−Trp distance of the $LiClO_4$ MG state.

The Soret CD spectrum (400−450 nm) is directly related to the structure of the heme pocket, and the Cotton effect at 416 nm is a probe for measuring the environment near the Met80−Fe(III) axial bond (*8*). Measurements of $[\theta]_{416}$ of cyt *c* in the acid MG state and D state (*8*) suggested that there is a gain of 67% in the Met80−Fe(III) intermediate during folding from the completely unstructured (D) state to MG states. We have measured Soret CD spectra of the $LiClO_4$-induced and LiCl-induced MG and D states of cyt *c* and estimated values of $[\theta]_{416}$ for both states produced by each denaturant (see Table 2). It has been observed that there are 44% and 68% gain in the Met80−Fe(III) ligation during folding from D to MG states in the cases of $LiClO_4$ and LiCl, respectively. These findings led us to conclude (i) that the ligation state of Fe(III)−Met80 seems to be same in the LiCl-induced and acid-induced MG states and (ii) that the Fe(III)−Met80 bond is more extended than the other MG states.

The radii of gyration of various MG states of cyt *c* are given in Table 2. It is seen in this table that R_G of the $LiClO_4$-induced MG state is larger than those obtained in other experimental conditions. This comparison suggests that the former is less compact than other MG states. Thus, this and other pieces of evidence presented above led us to conclude that the $LiClO_4$-induced MG state has different structural characteristics than those induced by LiCl at pH 6.0 and 0.25 M NaCl at pH 2.0. Why is the $LiClO_4$-induced MG state different from others? According to the Hoffmeister series, ClO_4^- binds to proteins and chloride is excluded from the protein surface (*35*). It is known that cosolutes, which are preferentially excluded, do not perturb protein structure, whereas preferentially binding cosolutes disrupt the structure of the protein (*36*−*38*). Indeed perchlorate is shown to bind cyt *c* (*39*−*41*). This binding to the MG state may exert steric hindrance leading to a more expanded MG state than those induced by Cl^- in the presence of LiCl, $CaCl_2$, and low pH (*10*).

In order to see whether the structurally different MG states have different stabilities, we have carried out measurements of transitions between the native and molten globule ensembles (transition I) and between the molten globule and denatured ensembles (transition II), and these transitions were analyzed for ΔG_D. A few comments are, however, necessary. First, each transition was analyzed for $\Delta G°$ values, assuming that $LiClO_4$-induced denaturation follows a two-state mechanism. One of the criteria to test the validity of a two-state assumption is to see whether one gets comparable values of thermodynamic parameters associated with the transition curves monitored by different structural probes. It can be seen in Figure 2B that, for each transition, values of fraction (*f*) and ΔG from different optical methods fall on the same *f* versus $[LiClO_4]$ and ΔG versus $[LiClO_4]$ plots, suggesting

that a two-state assumption seems to be valid. A more authentic test for the validity of the two-state assumption is to compare the total Gibbs free energy change associated with transitions I and II observed here with that from the DSC measurements for a two-state N ↔ D transition. It is interesting to note that the value of calorimetric Gibbs free energy change (ΔG^0_{N-D}) for the N ↔ D transition, which is 10 ± 1 kcal mol^{-1} (*42*), is in excellent agreement with that ($\Delta G_I^0 + \Delta G_{II}^X$) obtained from optical methods (see Table 1). This agreement between the thermodynamic parameter obtained from DSC and optical measurements also led us to believe that our analysis of thermodynamic parameters is authentic, and each process (transition I and transition II) follows a two-state mechanism. Second, it has been assumed that ΔG_I and ΔG_{II} vary linearly with [$LiClO_4$]. At present we do not have data to validate this assumption. However, it has been shown earlier (*10*) that plots of ΔG_I and ΔG_{II} versus [LiCl] and [$CaCl_2$] are linear.

Another assumption in the analysis of transition curves is that the thermodynamic characteristics of N, MG (X), and D ensembles are denaturant concentration-independent in the entire $LiClO_4$ concentration range. As shown by Bolen and co-workers (*43*, *44*), if this is not the case, i.e., cyt *c* exhibits "variable" thermodynamic character in its native, molten globule and denatured ensembles within and/or outside the transition zone, ΔG obtained from our analysis will be a complex quantity representing a continuum of reactions. As pointed out earlier (*43*), a direct demonstration of the $LiClO_4$-induced denaturation of cyt *c* representing a case of "fixed" thermodynamic characters of the N, X (MG), and D ensembles is to show that the sum of model-dependent Gibbs energies ΔG_I^0 and ΔG_{II}^X given in Table 2 is equal to ΔG_{N-D} obtained from the model-independent DSC measurements (*42*). Our assumption regarding the [$LiClO_4$]-independent thermodynamic characters of N, MG (X), and D ensembles is valid, for ΔG_{N-D}^0 ($= 10 \pm 1$ kcal mol^{-1} for N ↔ D) = ΔG_I ($= 9.5 \pm 0.1$ kcal mol^{-1} for N ↔ X) + ΔG_{II}^X ($= 1.3 \pm 0.2$ kcal mol^{-1} for X↔D).

It is seen in Table 2 that the Gibbs energy change is, within experimental error, the same for transitions between the N state and different MG states. It can also be seen in this table that about 86% of the total Gibbs energy change is associated with the N ↔ X transition. This is an important observation, for it suggests that the stability of the native protein is mainly due to interactions that are absent in the MG state. As discussed above, the MG state of cyt *c* is devoid of tight packing of the hydrophobic side chains, which play a role in the stabilization of the native state (*45*). It has been shown that the covalently bound heme interacts with about 35% of the buried side chains (*46*), and removal of heme from cyt *c* leads to unfolding of the polypeptide backbone (*47*). Thus, the packing of hydrophobic side chains and heme play a dominant role in stabilizing the native state of cyt *c*. Furthermore, contribution to the native stability due to the presence of secondary structure seems to be very small (see Table 2). Although the MG state induced by $LiClO_4$ is structurally different from those induced by LiCl and NaCl, they have the same thermodynamic stability (Table 2). We do not have any explanation of this unusual observation, namely, that the structurally different MG states have similar thermodynamic stability. It is noteworthy that Santucci et al. (*8*) have shown that at low pH $LiClO_4$-induced and NaCl-induced MG states have different structural characteristics but they have the same thermodynamic stability.

In summary, our in vitro study shows that cyt *c* has more than one MG states on its folding/unfolding pathway, and these MG states have the same thermodynamic stability in terms of ΔG but different flexibility.

ACKNOWLEDGMENT

We thank Prof. Yoji Goto (Institute for Protein Research, Osaka University, Japan) for his insight and comments. We also thank Professor M. A. Baig (Hamdard University, New Delhi, India) for his help with the fluorescence measurements.

REFERENCES

1. Dong, A., and Lam, T. (2005) Equilibrium titrations of acid-induced unfolding-refolding and salt-induced molten globule of cytochrome*c* by FT-IR spectroscopy, *Arch. Biochem. Biophys. 436*, 154−160.
2. Kumar, T. K. S., Subbiah, V., Ramakrishna, T., and Pandit, M. W. (1994) Trichloroacetic acid-induced unfolding of bovine pancreatic ribonuclease. Existence of molten globule-like state, *J. Biol. Chem. 269*, 12620−12625.
3. Mayouschek, A., Serrano, L., Meiering, E. M., Bycroft, M., and Ferscht, A. R. (1992) The folding of an enzyme. V. H/2H exchange-nuclear magnetic resonance studies on the folding pathway of barnase: complementarity to and agreement with protein engineering studies, *J. Mol. Biol. 224*, 837−845.
4. Barrick, D., Hughson, F. M., and Baldwin, R. L. (1994) Molecular mechanisms of acid denaturation. The role of histidine residues in the partial unfolding of apomyoglobin, *J. Mol. Biol. 237*, 588−593.
5. Arai, M., and Kuwajima, K. (2000) Role of molten globule state in protein folding, *Adv. Protein Chem. 53*, 209−271.
6. Ptitsyn, O. B. (1995) Molten globule and protein folding, *Adv. Protein Chem. 47*, 83−229.
7. Marmorino, J. L., Lehti, M., and Pielak, G. J. (1998) Native tertiary structure in an A-state, *J. Mol. Biol. 275*, 379−388.
8. Santucci, R., Bongiovanni, C., Mei, G., Ferri, T., Polizio, F., and Desideri, A. (2000) Anion size modulates the structure of the A state of cytochrome*c*, *Biochemistry 39*, 12632−12638.
9. Goto, Y., Takahashi, N., and Fink, A. L. (1990) Mechanism of acid-induced folding of proteins, *Biochemistry 29*, 3480−3488.
10. Qureshi, S. H., Moza, B., Yadav, S., and Ahmad, F. (2003) Conformational and thermodynamic characterization of the molten globule state occurring during unfolding of cytochromes *c* by weak salt denaturants, *Biochemistry 42*, 1684−1695.
11. Tcherkasskaya, O., and Ptitsyn, O. B. (1999) Molten globule versus variety of intermediates: influence of anions on pH-denatured apomyoglobin, *FEBS Lett. 455*, 325−331.
12. Sinibaldi, F., Howes, B. D., Smulevich, G, Ciaccio, C., Coletta, M., and Santucci, R. (2003) Anion concentration modulates the conformation and stability of the molten globule of cytochrome*c*, *J. Biol. Inorg. Chem. 8*, 663−670.
13. Chalikian, T. V., Gindikin, V. S., and Breslauer, K. J. (1996) Spectroscopic and volumetric investigation of cytochrome*c* unfolding at alkaline pH: characterization of base-induced unfolding state at 25 °C, *FASEB 10*, 164−170.
14. Bongiovanni, C., Sinibaldi, F., Ferri, T., and Santucci, R. (2002) Glycerol-induced formation of the molten globule from acid-denatured cytochrome*c*: implication for hierarchical folding, *J. Protein Chem. 21*, 35−41.
15. Tsong, T. Y.(1975) An acid induced conformational transition of denatured cytochrome c in urea and guanidine hydrochloride, *Biochemistry 14*, 1542−1547.
16. Margoliash, E., and Forhwirt, N. (1959) Spectrum of horse heart cytochrome*c*, *Biochem. J. 71*, 570−572.
17. Mulqueen, P. M., and Kronman, M. J. (1982) Binding of naphthalene dyes to the N and A conformers of bovine alpha-lactalbumin, *Arch. Biochem. Biophys. 215*, 28−39.
18. Ahmad, F., and Bigelow, C. C. (1982) Estimation of free energy of stabilization of ribonuclease-A, lysozyme, alpha-lactalbumin and myoglobin, *J. Biol. Chem. 257*, 12935−12940.

19. Ahmad, F., and Salahuddin, A. (1974) Influence of temperature on the intrinsic viscosities of proteins in random coil conformation, *Biochemistry 13*, 245−249.
20. Stellwagen, E. (1968) The reversible unfolding of horse cytochrome*c*, *Biochemistry 7*, 2893−2898.
21. Ohgushi, M., and Wada, A. (1983) Molten globule state: a compact form of globular proteins with mobile side chains, *FEBS Lett. 164*, 21−24.
22. Kataoka, M., Hagihara, Y., Mihara, K., and Goto, Y. (1993) Molten globule of cytochrome *c* studied by the small angle X-ray scattering, *J. Mol. Biol. 229*, 591−596.
23. Jeng, M. F., Englander, S. W., Elöve, G. A., Wand, A. J., and Roder, H. (1990) Structural description of acid-denatured cytochrome c by hydrogen exchange and 2D NMR, *Biochemistry 29*, 10433−10437.
24. Colon, W., and Roder, H. (1996) Kinetic intermediates in the formation of the cytochrome*c* molten globule, *Nat. Struct. Biol. 3*, 1019−1025.
25. Kuroda, Y., Kidokoro, S., and Wada, A. (1992) Thermodynamic characterization of cytochrome *c* at low pH: observation on the molten globule state and of the cold denaturation process, *J. Mol. Biol. 223*, 1139−1153.
26. Grandori, R. (2002) Detecting equilibrium cytochrome *c* folding intermediates by electrospray ionisation mass spectrometry: two partially folded forms populate the molten globule state, *Protein Sci. 11*, 453−458.
27. Ali, V., Prakash, K., Kulkarni, S., Ahmad, A., Madhusudan, K. P., and Bhakuni, V. (1999) 8-Anilino-1-naphthalene sulfonic acid (ANS) induces folding of acid unfolded cytochrome*c* to molten globule state as a result of electrostatic interactions, *Biochemistry 38*, 13635−13642.
28. Tanford, C. (1961) *Physical Chemistry of Macromolecule*, Wiley, New York.
29. Davis-Searles, P. R., Morar, A. S., Saunderes, A. J., Erie, D. A., and Pielak, G. J. (1998) Sugar induced molten globule model, *Biochemistry 37*, 17048−17053.
30. Konno, T. (2001) Multistep nucleus formation and a separate subunit contribution of the amyloidgenesis of heat-denatured monellin, *Protein Sci. 10*, 2093-2101.
31. Bai, Y., Sosnick, T. R., Mayne, L., and Englander, S. W. (1995) Protein folding intermediates: native-state hydrogen exchange, *Science 269*, 192−197.
32. Marmorino, J. L., and Pielak, G. J. (1995) A native tertiary interaction stabilizes the A state of cytochrome *c*, *Biochemistry 34*, 3140−3143.
33. Dill, K. A., and Chan, H. S. (1997) From Levinthal to pathways to funnels, *Nat. Struct. Biol. 4*, 10−19.
34. Yeh, S. R., and Rousseau, D. L. (1999) Ligand exchange during unfolding of cytochrome *c*, *J. Biol. Chem. 274*, 17853−17859.
35. Collins, K. D., and Washabaugh, M. W. (1985) The Hofmeister effect and the behavior of water at interfaces, *Q. Rev. Biophys. 18*, 323−422.
36. Timasheff, S. N. (2002) Protein−solvent preferential interactions, protein hydration, and the modulation of biochemical reactions by solvent components, *Proc. Natl. Acad. Sci. U.S.A. 99*, 9721−9726.
37. Schellman, J. A. (2002) Fifty years of solvent denaturation, *Biophys. Chem. 96*, 91−101.
38. Wyman, J., Jr. (1965) The binding potential, a neglected linkage concept, *J. Mol. Biol. 11*, 631−644.
39. Thomas, A., Jonas, A., Karl-Erik, F., and Sture, F. (1980) Perchlorate binding to cytochrome*c*: a magnetic and optical study, *Eur. J. Biochem. 110*, 363−369.
40. Lindman, B., and Forsen, S. (1976) *Physico-Chemical and Biological Applications*, Springer-Verlag, Heidelberg.
41. Battostizzo, G., Borsari, M., Dallari, D., Lancellotti, I., and Sola, M. (1996) Anion binding to mitochondrial cytochromes *c* studied through electrochemistry: effects of the neutralization of surface charges on the redox potential, *Eur. J. Biochem. 241*, 208−214.
42. Makhatadze, G. I., Clore, G. M., and Groneborn, A. M. (1995) Solvent isotope effect and protein stability, *Nat. Struct. Biol. 2*, 852−855.
43. Bolen, D. W., and Yang, M. (2000) Effect of guanidine hydrochloride on the proton inventory of proteins: Implications on interpretations of protein stability, *Biochemistry 39*, 15208−15216.
44. Ferreon, A. C., and Bolen, D. W. (2004) Thermodynamics of denaturant-induced unfolding of a protein that exhibits variable two-state denaturation, *Biochemistry 43*, 13357−13369.
45. Barrick, D., and Baldwin, R. L. (1993) The molten globule intermediate of apomyoglobin and the process of protein folding, *Protein Sci. 2*, 869−876.
46. Dickerson, R. E., Takano, T., Eisenberg, D., Kallia, O. B., Samson, L., Cooper, A., and Margoliash, E. (1971) Ferricytochrome*c* 1. General features of horse and bovine proteins at 2.8 Å resolution, *J. Biol. Chem. 246*, 1511−1535.
47. Fisher, W. R., Taniuchi, H., and Anfinsen, C. B. (1973) The role of heme in the formation of the structure of cytochrome*c*, *J. Biol. Chem. 248*, 3188−3195.

BI052357R